

# Hydrodynamic interactions in DNA thermophoresis

Aboubakry Ly and Alois Würger

*Laboratoire Ondes et Matière d'Aquitaine, Université de Bordeaux & CNRS, 33405 Talence, France*

We theoretically study the molecular-weight dependence of DNA thermophoresis, which arises from mutual advection of the  $n$  repeat units of the molecular chain. As a main result we find that the dominant driving forces, i.e., the thermally induced permittivity gradient and the electrolyte Seebeck effect, result in characteristic hydrodynamic screening. In comparison with recent experimental data on single-stranded DNA ( $2 \leq n \leq 80$ ), our theory provides a good description for the increase of the drift velocity up to  $n = 30$ ; the slowing-down of longer molecules is well accounted for by a simple model for counterion condensation. It turns out that thermophoresis may change sign as a function of  $n$ : For an appropriate choice of the salt-specific Seebeck coefficient, short molecules move to the cold and long ones to the hot; this could be used for separating DNA by molecular weight.

PACS numbers:

When applying a temperature gradient on a colloidal dispersion, one observes thermally driven transport towards the hot or the cold [1, 2]. In recent years, thermophoresis has been shown to provide a versatile means for manipulating DNA, including translocation through plasmonic nanopores [3], stretching in nanochannels [4, 5], separation by molecular weight [6], sequence-specific detection with functionalized nanoparticles [7], and force-free trapping of single molecules [8]. Protein thermophoresis has become a standard technology in biomedical analysis [9], and the accumulation of RNA in hydrothermal pores is discussed as a scenario for biomolecular synthesis in the early evolution of life [10].

In the last decade, much progress has been made concerning the physical mechanisms of thermophoresis of charged colloids. It has been shown that, in addition to thermo-osmosis [11, 12], the electrolyte Seebeck field [13–18] and concentration gradients of salt [16] or non-ionic polymers [19, 20], play an important role. These companion fields arise from specific solvation enthalpies of salt ions or nonionic solutes, and are at the origin of the “inverse” Soret effect, where the colloids accumulate in hot regions [16, 19]. Regarding the size dependence, there is conclusive evidence that the mobility of colloidal beads does not vary with the radius [21, 22].

In spite of the many experimental studies mentioned above, little is known on the molecular-weight dependence of DNA thermophoresis. If the hydrodynamic slowing-down of Brownian motion is well understood in terms of mutual advection of the repeat units [23], a more complex picture arises for phoretic motion where external forces are absent and which is driven by non-equilibrium surface properties. For short-ranged dispersion forces, hydrodynamic interactions are irrelevant and the thermophoretic velocity is constant [24, 25]; deviations observed for very short polymers in organic solvents [26], arise probably from chemically different end groups. For DNA in a weak electrolyte, however, the electrostatic interaction length may attain tens of nanometers, which suggests an incomplete screening of hydrodynamic cou-

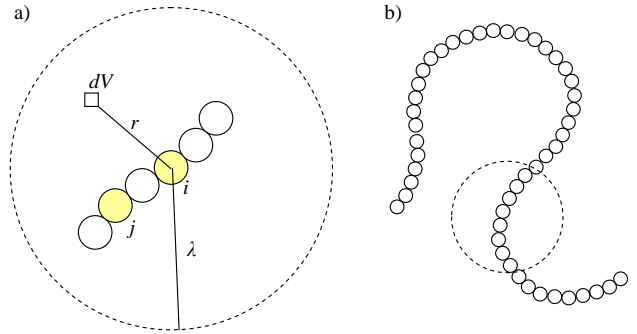


FIG. 1: Schematic view of a charged polymer in an electrolyte solution. a) The drag on the molecular unit  $j$  consists of two contributions: First, the Stokeslet of bead  $i$ , driven by the force  $\mathbf{F}$ , drags the neighbor  $j$ . Second, due to the force  $\mathbf{f}(\mathbf{r})$  exerted by the bead  $i$ , the fluid element  $dV$  moves and in turn exerts a drag on bead  $j$ . These contributions cancel each other at distances well beyond the Debye length  $\lambda$ . b) Since the persistence length is of the order of the Debye length, the molecule may be treated as a rigid rod within the reach of electrostatic interactions.

pling.

In this paper we study hydrodynamic effects on DNA thermophoresis. We consider the two dominant charge-related surface forces, i.e., the thermally induced permittivity gradient and the electrolyte Seebeck effect, and derive the respective hydrodynamic correction factors in the rigid-rod limit. With a simple model for counterion condensation, we compare our theory to recent Soret data for single-stranded DNA [17].

*Hydrodynamic interactions.* – Consider a polyelectrolyte chain of  $n$  building blocks, as illustrated in Fig. 1. Unit  $i$  creates a flow field  $\mathbf{v}(\mathbf{r} - \mathbf{r}_i)$  in the surrounding fluid and thus drags its neighbor  $j$ . Then the overall velocity  $\mathbf{u}$  of the chain is given by the sum of the monomer

contribution  $\mathbf{u}_1$  and the mutual advection,

$$\mathbf{u} = \mathbf{u}_1 + \frac{1}{n} \sum_{i,j \neq i} \langle \mathbf{v}(\mathbf{r}_{ij}) \rangle, \quad (1)$$

where the angular brackets  $\langle \cdot \cdot \rangle$  indicates the configurational average with respect to  $\mathbf{r}_{ij} = \mathbf{r}_j - \mathbf{r}_i$ .

Thermophoresis arises from the solute-solvent interactions. The force density exerted on the counterion cloud surrounding a charged monomer reads as [27]

$$\mathbf{f} = -\frac{E^2}{2} \nabla \epsilon + \rho \mathbf{E}_T, \quad (2)$$

where the first term is proportional to the thermally induced permittivity gradient  $\nabla \epsilon = (d\epsilon/dT) \nabla T$ , with the charged monomer's electric field  $E$ . Since the permittivity decreases with rising temperature,  $d\epsilon/dT < 0$ , the surrounding water moves to the hot, as recently confirmed experimentally for thermoosmosis in a capillary [12]. By reaction, the molecule migrates toward the cold.

The second term in (2) describes the force exerted by the macroscopic thermoelectric field  $\mathbf{E}_T = S \nabla T$  on the monomer's counterion density  $\rho$  [14]. The electrolyte Seebeck coefficient  $S$  is a salt-specific quantity that may take either sign, resulting in motion along the temperature gradient or opposite to it [16]. Eq. (2) gives the dominant thermal forces to leading order in the ratio  $a/\lambda$  of the monomer radius and the Debye length. Additional companion fields, such as the salinity gradient, arise in the colloid limit where  $a$  is comparable to or larger than  $\lambda$  [16].

The force density  $\mathbf{f}$  acts on the surrounding water and, by reaction, the molecular unit is subject to the opposite force  $\mathbf{F} = -\int dV \mathbf{f}$  [27]. Thus the velocity field induced by the moving bead  $i$  at the position of its neighbor  $j$ , consists of two contributions,

$$\mathbf{v}(\mathbf{r}_{ij}) = \mathbf{G}(\mathbf{r}_{ij}) \cdot \mathbf{F} + \int \mathbf{G}(\mathbf{r}_{ij} - \mathbf{r}) \cdot \mathbf{f}(\mathbf{r}) dV, \quad (3)$$

where  $\mathbf{G}(\mathbf{r}) = (1 + \widehat{\mathbf{r}}\widehat{\mathbf{r}})/8\pi\eta r$  is the Oseen tensor with the viscosity  $\eta$  and  $\widehat{\mathbf{r}} = \mathbf{r}/r$  [28]. The first term describes the long-range velocity field  $v \sim 1/r_{ij}$  or "stokeslet" of particle  $i$  at the position  $j$ , due to the force  $\mathbf{F}$ ; it gives rise to strong hydrodynamic effects on diffusion and sedimentation [23]. The second term is characteristic for phoretic motion; it may be viewed as the sum of stokeslet flows of strength  $\mathbf{f}dV$  and centered at a distance  $\mathbf{r}$  from particle  $i$ , as illustrated in Fig. 1a. Since both  $E$  and  $\rho$  vanish well beyond the Debye length, the second term cancels the first one at large distances,  $r_{ij} \gg \lambda$ , whereas it is small for nearby beads.

As a consequence of this hydrodynamic screening, the advection velocity (3) varies as  $1/r_{ij}$  within the Debye length but vanishes at larger distances. When performing the configurational average in (1) with the (isotropic) equilibrium distribution function, the only finite component of the mean drag velocity is along the force density  $\mathbf{f}$ ,

that is, along the temperature gradient. Then the tensor equation simplifies to a scalar one, and Eq. (1) becomes

$$u = u_1 + \frac{1}{n} \sum_{i,j \neq i} \int \langle G(|\mathbf{r}_{ij} - \mathbf{r}|) - G(r_{ij}) \rangle f(\mathbf{r}) dV, \quad (4)$$

with the Oseen tensor replaced by its diagonal part  $G(r) = 1/6\pi\eta r$ . This form shows that mutual advection vanishes for distant pairs with  $r_{ij} \gg \lambda$ , thus nicely displaying hydrodynamic screening.

In order to evaluate (4) we need to explicit the force density  $f(\mathbf{r})$ . The electrostatic potential of a single bead of valency  $\hat{z}$  is well described by the Debye-Hückel expression

$$\psi = -\frac{\hat{z}e}{4\pi\epsilon r} e^{-r/\lambda} = \zeta_1 \frac{a}{r} e^{-r/\lambda}, \quad (5)$$

where the second equality defines the single-bead surface potential  $\zeta_1 = -\hat{z}e/4\pi\epsilon a$ , which we assume to be negative. One readily obtains the radial electric field  $E = -d\psi/dr$  and the counterion charge density  $\rho = -\epsilon\psi/\lambda^2$  which determine the force density (2). Then the volume integrals in (4) can be performed in closed form [29], resulting in the factors  $\langle e^{-2r_{ij}/\lambda}/r_{ij}^2 \rangle$  and  $\langle e^{-r_{ij}/\lambda}/r_{ij} \rangle$ . Since the main contribution to Eq. (4) stems from within the screening length  $\lambda$ , which in turn is comparable to the molecular persistence length [30], the chain may be treated as rigid such that the distance of beads  $i, j$  simplifies to  $r_{ij} = |i - j|d$ . Replacing moreover the double sum by integrals over  $i$  and  $j$ , we obtain

$$\mathbf{u} = \frac{\zeta_1^2}{3\eta} (1 + \chi_\epsilon) \nabla \epsilon + \frac{2\epsilon\zeta_1}{3\eta} (1 + \chi_S) \mathbf{E}_T, \quad (6)$$

where the quantities  $\chi_\epsilon$  and  $\chi_S$  account for hydrodynamic interactions (see Fig. 2.) With  $\chi_\epsilon = 0 = \chi_S$  one has the explicit expression for the monomer velocity  $\mathbf{u}_1$  defined in (1).

The hydrodynamic correction factor for motion driven by the permittivity gradient reads

$$\chi_\epsilon = \frac{a^2}{d^2} \left( (1 + 2n\hat{d}) \frac{E_{2\hat{d}} - E_{2n\hat{d}}}{n} + e^{-2\hat{d}} - \frac{e^{-2n\hat{d}}}{n} \right), \quad (7)$$

with the shorthand notation  $E_x = \text{Ei}(-x)$  for the exponential integral function, and  $\hat{d} = d/\lambda$  for the ratio of the monomer length and the Debye length. For the Seebeck term we find

$$\chi_S = \frac{2a}{d} \left( E_{n\hat{d}} - E_{\hat{d}} + \frac{e^{-n\hat{d}} - e^{-\hat{d}}}{n\hat{d}} \right), \quad (8)$$

The factor 2 in the exponential and Ei functions in  $\chi_\epsilon$  arises from the screening factor of the force density,  $E^2 \propto e^{-2r/\lambda}$ , whereas the factors in  $\chi_S$  are related to the decay of the screening cloud,  $\rho \propto e^{-r/\lambda}$ . Fig. 2 shows  $\chi_\epsilon$  and  $\chi_S$  as a function of the molecular weight. Both vanish for monomers,  $n = 1$ , whereas for long molecules they

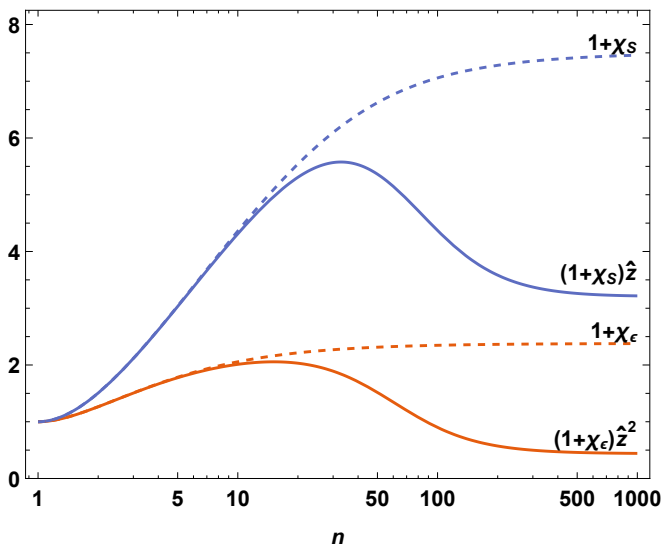


FIG. 2: Molecular-weight dependence of the two contributions to  $D_T$ . Both hydrodynamic factors  $\chi_\epsilon$  and  $\chi_S$  increase with  $n$ , albeit with different amplitudes, as shown by the dashed lines; the parameters are the monomer distance  $d = 3\text{\AA}$  and the Debye length  $\lambda = 5\text{ nm}$ . Counterion condensation results in the factors  $\hat{z}^2$  and  $\hat{z}$ , which significantly reduce the mobility (solid lines), according to (9) with  $\beta_n = (n^2 - 1)n_0^{-2}$  and  $n_0 = 80$ .

tend toward the constants  $\chi_\epsilon^\infty = (a/d)^2(2\hat{d}E_{2\hat{d}} + e^{-2\hat{d}})$  and  $\chi_S^\infty = -2(a/d)E_{\hat{d}}$ . Note that  $\chi_S$  is identical to the hydrodynamic correction of electrophoresis [31]. Flexible molecules, such as the bead-spring model, would result in cumbersome formal expressions without changing the qualitative features. For example, evaluating the configuration average with a power law for the bead-bead distance,  $\langle r_{ij}^2 \rangle \propto |i - j|^{2\nu}$ , results in an incomplete Gamma function  $\Gamma(\nu^{-1}, nd/\lambda)$  instead of an exponential integral; the numerical evaluation of the mean velocity (4) hardly differs from the above correction factors.

*Counterion condensation.*— A polyelectrolyte carries a line charge  $e/d$ . If the bead spacing  $d$  is larger than the Bjerrum length  $l_B \approx 7\text{\AA}$ , Debye-Hückel approximation is valid even for long chains, and the electrostatic potential reads  $\sum_i \psi_i(\mathbf{r} - \mathbf{r}_i)$ . Yet in the opposite case  $d < l_B$ , which is relevant for DNA, this linear superposition ceases to be valid as  $n$  increases. Because of the strong Coulomb interaction, the counterions partly condense onto the polymer until its linear charge density is reduced to the critical value  $e/l_B$  [32]. The remaining free counterions are well described by Debye-Hückel theory.

In a mean-field model, counterion condensation is described by an effective valency

$$\hat{z} = \xi^{-1} + \frac{1 - \xi^{-1}}{1 + \beta_n}, \quad (9)$$

where  $\xi = l_B/d > 1$  is the Manning parameter. For a monomer the quantity  $\beta_1$  vanishes, and one has  $\hat{z} = 1$ . For long chains,  $\beta_n$  tends to infinity, thus resulting in

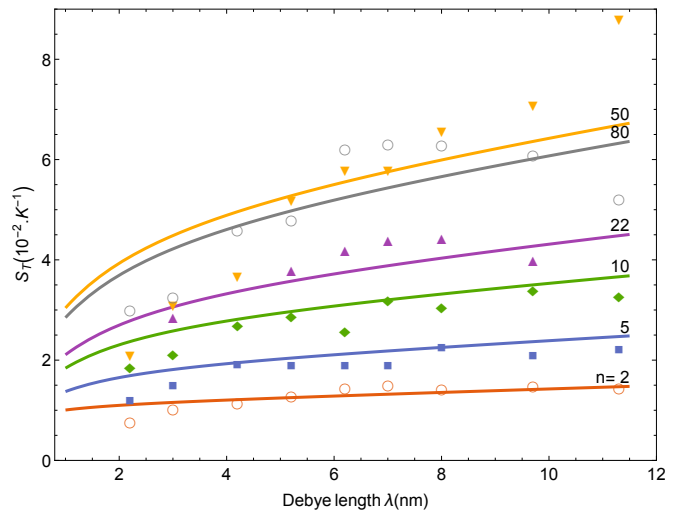


FIG. 3: The Soret coefficient  $S_T$  as a function of the Debye length  $\lambda$  for DNA of different length  $n$ . The data points, measured at  $15^\circ\text{C}$ , are taken from Ref. [17]. The theory curves are calculated from  $S_T = D_T/D$ , where  $D_T$  is given by Eq. (10) with  $\hat{S} = 0$ ,  $a = 4.25\text{\AA}$ , and  $d = 3\text{\AA}$ . The values of the diffusion coefficient  $D$  for  $n = 5, \dots, 50$  are obtained from experiment [17], those for  $n = 2$  and  $80$  are extrapolated from the previous and from the power law for long molecules [35].

$\hat{z} = \xi^{-1}$  and reducing the charge density to its critical value  $\hat{z}e/d = e/l_B$  [32]. The progressive condensation of the counterions on the chain, and the dependence of  $\beta_n$  on  $n$  and  $\lambda$ , constitute an intricate problem which is beyond the scope of the present paper [33]. Here we use the simple form  $\beta_n = (n^2 - 1)n_0^{-2}$  which, with  $n_0 = 80$ , fits rather well the experimental data. Note that this model does not depend on the electrolyte strength.

*Phoretic coefficients.*— The thermophoretic mobility is defined through the drift velocity  $u = -D_T \nabla T$  in a temperature gradient. From (6) we find

$$D_T = \frac{k_B}{12\pi\eta a} \left( \frac{l_B}{a} \hat{z}^2 (1 + \chi_\epsilon) \tau + 2\hat{z} (1 + \chi_S) \hat{S} \right), \quad (10)$$

with the parameter  $\tau = -d \ln \epsilon / d \ln T \approx 1.4$  which arises from the permittivity gradient, and the dimensionless Seebeck coefficient  $\hat{S} = S(e/k_B)$ . For monomers the mobility is independent of the Debye length, whereas for longer chains, the correction factors give rise to complex dependencies on  $\lambda$  and  $n$ . In Fig. 2 we plot the two contributions to  $D_T$  as a function of  $n$ . The initial increase results from hydrodynamic interactions (dashed lines), whereas the decrease at larger  $n$  is due to counterion condensation (solid lines). Both factors reach a finite value at large  $n$ ; for typical parameters of DNA in a weak electrolyte, the permittivity term shows an overall decrease,  $\hat{z}^2(1 + \chi_\epsilon^\infty) < 1$ , whereas the Seebeck term is enhanced,  $\hat{z}(1 + \chi_S^\infty) > 1$ .

The stationary DNA concentration  $c$  is achieved when thermophoretic drift and gradient diffusion with coefficient  $D$  cancel each other,  $cu - D\nabla c = 0$ . This ‘‘Soret

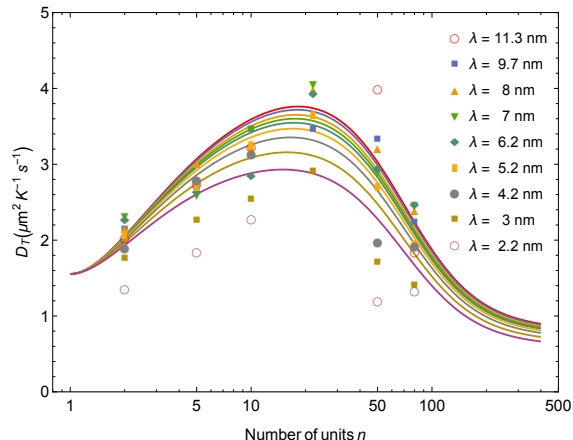


FIG. 4: Thermophoretic mobility  $D_T$  as a function of the molecular length  $n$  for various values of the Debye length  $\lambda$ . The full curves are calculated from Eq. (10) with  $\hat{S} = 0$ ,  $a = 4.25\text{\AA}$  and  $d = 3\text{\AA}$ . The data points give  $D_T = DS_T$ , with  $S_T$  and the hydrodynamic radius from Ref. [17]; for details see [29].

equilibrium” is usually written in the form  $\nabla c + cS_T \nabla T = 0$ , since experiments probe the Soret coefficient  $S_T = D_T/D$  rather than the mobility  $D_T$ . In Fig. 3 we compare our theory with Soret data for single-stranded DNA as a function of the Debye length  $\lambda$ , taken from Ref. [17]. The theoretical curves are calculated with (10) and a simple model for the measured diffusion coefficient  $D$ , as described in [29]. The best agreement with the data is obtained when retaining in (10) the permittivity-gradient term only, that is, for zero Seebeck coefficient,  $\hat{S} = 0$ . The increase of  $S_T$  with the Debye length arises mainly from the hydrodynamic correction  $\chi_\epsilon$ . For short chains,  $n < 30$ , the variation with  $n$  is of purely hydrodynamic origin, whereas for larger chains counterion condensation plays an important role, as is clear from Fig. 2.

In order to clearly display the effect of hydrodynamic interactions, we plot in Fig. 4 the thermophoretic mobility (10) as a function of the molecular weight  $n$ . The experimental points are obtained from  $D_T = DS_T$ , with measured  $S_T$  and  $D$  [17] as described in [29]. The theoretical curves are calculated with the permittivity-gradient only ( $\hat{S} = 0$ ). The initial increase of the data up to  $n = 22$  agrees well with the relation (7), thus providing strong evidence for the role of hydrodynamic interactions. The maximum and the subsequent decrease are well described by counterion condensation according to (9). Adding a significant thermoelectric contribution would not improve the quality of the fit, quite on the contrary. This suggests that the Seebeck field in NaCl solution is small, confirming a previous analysis of Soret data for polystyrene beads [16].

The electrolyte Seebeck effect was discarded in the

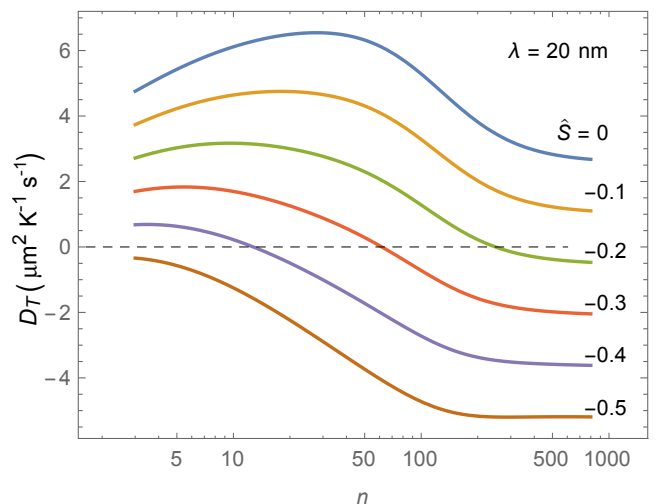


FIG. 5: Thermophoretic mobility  $D_T$  as a function of the chain length  $n$ , for different values of the dimensionless Seebeck coefficient  $\hat{S}$ . For negative  $\hat{S}$  the thermoelectric field in (6) drives the molecules toward the hot, whereas the permittivity gradient points toward the cold. Since the latter dominates for short molecules and the latter for long ones,  $D_T$  changes sign as the  $n$  increases.

above analysis of Soret data in NaCl solution. In Fig. 5 we plot the complete mobility  $D_T$  as a function of  $n$ , for several values of the dimensionless Seebeck coefficient  $\hat{S}$ . As the most striking feature, for negative  $\hat{S}$  the superposition of the two contributions in (10) may result in a change of sign of the  $D_T$ . From Fig. 2 it is clear that for short chains, the permittivity gradient term prevails, whereas for longer molecules the Seebeck term dominates because of its much larger hydrodynamic factor  $\chi_S$ .

The resulting velocity difference could be used for specific accumulation of one component at a heated spot, or for separating DNA by molecular size. For example, in an electrolyte with  $\hat{S} = -0.3$ , the permittivity-gradient term dominates for short molecules ( $n < 50$ ) which move to the cold accordingly, whereas longer chains ( $n > 50$ ) are driven to the hot by the thermoelectric field  $E_T$ . The stagnation molecular length  $n_c$ , where  $D_T = 0$ , is easily adapted by choosing an appropriate salt mixture. The change of sign has been observed for nano-size micelles [15] and micron-size polystyrene beads [16] in mixed electrolytes  $\text{NaOH}_x\text{Cl}_{1-x}$ ; the values of  $\hat{S}$  used in Fig. 5 are realized by with  $0.1 < x < 0.4$ .

*Conclusion.* – We briefly summarize our main results on DNA thermophoresis. We find that DNA thermophoresis is rather sensitive to hydrodynamic interactions. With increasing chain length  $n$ , the mobility is enhanced due to mutual advection of the repeat units, then passes through a maximum, and finally decreases below the monomer value due to counterion condensation. Comparison with measured data in Fig. 4, provides strong evidence that the molecular-weight dependence

arises from the interplay of hydrodynamic interactions and non-linear charge effects. The interplay between the dominant driving forces, that is, the permittivity gradient and a thermoelectric field with negative Seebeck coefficient, results in a change of sign as a function of  $n$ :

Short molecules move to the cold, and long ones to the hot.

The authors acknowledge funding by the French National Research Agency through contract ANR-13-IS04-0003.

- 
- [1] R. Piazza, *Soft Matter* **4**, 1740 (2008).
- [2] A. Würger, *Rep. Prog. Phys.* **73**, 126601 (2010)
- [3] F. Nicoli, D. Verschuere, M. Klein, C. Dekker, and M.P. Jonsson, *Nano Lett.* **14**, 6917 (2014)
- [4] J.N. Pedersen, C.J. Lüscher, R. Marie, L.H. Thamdrup, A. Kristensen, and H. Flyvbjerg, *Rev. Lett.* **113**, 268301 (2014)
- [5] Y. He, M. Tsutsui, R.H. Scheicher, F. Bai, M. Taniguchi, and T. Kawai, *ACS Nano* **7**, 538 (2013)
- [6] Y.T. Maeda, A. Buguin, and A. Libchaber, *Phys. Rev. Lett.* **107**, 038301 (2011)
- [7] L.-H. Yu and Y.-F. Chen, *Anal. Chem.* **87**, 2845 (2015)
- [8] M. Braun, T. Thalheim, K. Günther, M. Mertig, and F. Cichos, *Proc. SPIE 9922, Optical Trapping and Optical Micromanipulation XIII*, 99220Z (2016)
- [9] M. Jerabek-Willemsen, T. Andréa, R. Wannera, H.M. Rotha, S. Duhr, Ph. Baaske, D. Breitsprecher, *J. Mol. Structure* **1077**, 101 (2014)
- [10] P. Baaske, F.M. Weinert, S. Duhr, K.H. Lemke, M.J. Russell, and D. Braun, *PNAS* **104**, 9346 (2007)
- [11] E. Ruckenstein, *J. Coll. Interf. Sci.* **83**, 77 (1981)
- [12] A.P. Bregulla, A. Würger, K. Günther, M. Mertig, and F. Cichos, *Phys. Rev. Lett.* **116**, 188303 (2016)
- [13] S.A. Putnam, D.G. Cahill, G.C.L. Wong, *Langmuir* **23**, 9221 (2007)
- [14] A. Würger, *Phys. Rev. Lett.* **101**, 108302 (2008)
- [15] D. Vigolo, S. Buzzaccaro and R. Piazza, *Langmuir* **26**, 7792 (2010).
- [16] K.A. Eslahian, A. Majee, M. Maskos, A. Würger, *Soft Matter* **10**, 1931 (2014)
- [17] M. Reichl, M. Herzog, A. Götz, and D. Braun, *Phys. Rev. Lett.* **112**, 198101 (2014)
- [18] S. Simoncelli, J. Summer, S. Nedev, P. Kühler, and J. Feldmann, *Small* **29**, 2854 (2016).
- [19] H.-R. Jiang, H. Wada, N. Yoshinaga and M. Sano, *Phys. Rev. Lett.* **102**, 208301 (2009)
- [20] T. Tsuji, K. Kozai, H. Ishino, and S. Kawano, *Micro & Nano Letters*, doi: 10.1049=mnll.2012.0357 (2017)
- [21] M. Braibanti, D. Vigolo, R. Piazza, *Phys. Rev. Lett.* **100**, 108303 (2008).
- [22] A. Würger, *Phys. Rev. Lett.* **116**, 138302 (2016)
- [23] P. -G. de Gennes, *Scaling concepts in Polymer Physics*, Cornell University Press: Ithaca (1979)
- [24] F. Brochard, P.-G. de Gennes, *C. R. Acad. Sc. Paris, Série II* **293**, 72 (1981)
- [25] S. Wiegand, *J. Phys. Cond. Matt.* **16**, 357 (2004)
- [26] D. Stadelmaier, W. Köhler, *Macromolecules* **41**, 6205 (2008)
- [27] J. Morthomas and A. Würger, *Eur. Phys. J.* **27**, 425-434 (2008)
- [28] S. Kim, S. J. Karilla, *Microhydrodynamic: Principles and Selected Applications*, Butterworth-Heinemann Boston (1991)
- [29] Details for the derivation of the thermophoretic mobility, the effective charge, and the experimental data and graphs are given in Supplementary Material.
- [30] B. Tinland, A. Pluen, J. Sturm, and G. Weill, *Macromolecules* **30**, 5763 (1997)
- [31] M. Muthukumar, *Macro. Theo. Simul.* **3**, 61-71 (1994)
- [32] G. S. Manning, *J. Chem. Phys.* **51**, 924 (1969) and *J. Phys. Chem.* **85**, 1508-1515 (1981)
- [33] K. Grass and C. Holm, *Faraday Discuss.* **144**, 57-70 (2010)
- [34] See Supplemental material for technical details
- [35] A. Sim, J. Lipfert, D. Herschlag, S. Doniach, *Phys. Rev. E.* **86**, 021901 (2012)